

A New Pathway to Approximate Energy Expenditure and Recovery of an Athlete—Appendix

Fabian Clemens Weigend
Fabian.Weigend@westernsydney.edu.au
Western Sydney University
Australia

Jason Siegler
Jason.Siegler@asu.edu
Arizona State University
USA

Oliver Obst
O.Obst@westernsydney.edu.au
Western Sydney University
Australia

ABSTRACT

This work proposes to use evolutionary computation as a pathway to allow a new perspective on the modeling of energy expenditure and recovery of an individual athlete during exercise.

We revisit a theoretical concept called the “three component hydraulic model” which is designed to simulate metabolic systems during exercise and which is able to address recently highlighted shortcomings of currently applied performance models. This hydraulic model has not been entirely validated on individual athletes because it depends on physiological measures that cannot be acquired in the required precision or quantity.

This paper introduces a generalized interpretation and formalization of the three component hydraulic model that removes its ties to concrete metabolic measures and allows to use evolutionary computation to fit its parameters to an athlete.

CCS CONCEPTS

• **Computing methodologies** → *Modeling methodologies; Model verification and validation; Simulation by animation.*

KEYWORDS

performance modeling, metabolic response modeling, optimization

ACM Reference Format:

Fabian Clemens Weigend, Jason Siegler, and Oliver Obst. 2021. A New Pathway to Approximate Energy Expenditure and Recovery of an Athlete—Appendix. In *2021 Genetic and Evolutionary Computation Conference Companion (GECCO '21 Companion)*, July 10–14, 2021, Lille, France. ACM, New York, NY, USA, 6 pages. <https://doi.org/10.1145/3449726.3459469>

APPENDIX

The main poster paper provides a concise description of our approach. We add this appendix to substantiate proposed theory and to ensure replicability. The implemented hydraulic model, an interactive simulation, and the outlined evolutionary fitting approach are available at https://github.com/faweigend/three_comp_hyd.

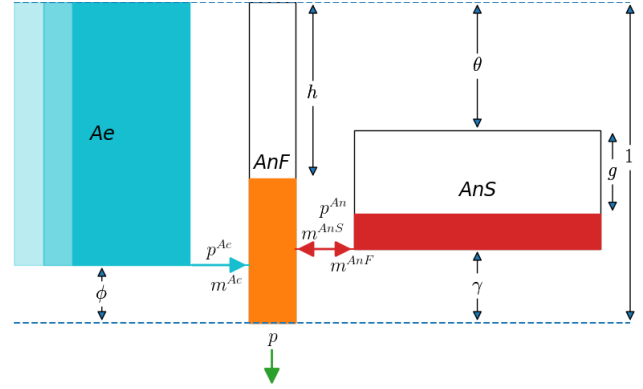


Figure 1: A generalized schematic of the three component hydraulic model. Tanks are renamed as aerobic component Ae, anaerobic fast component AnF and anaerobic slow component AnS. p^{Ae} and p^{An} represent flows and $-m^{AnF}$, m^{AnS} , and m^{Ae} maximal flow capacities.

A MODEL GENERALIZATION AND FORMALIZATION

Our generalized interpretation of the three component hydraulic model removes its ties to concrete physiological measures. This section defines this more general view with a robust formalization of its dynamics. These steps—generalization and formalization—ultimately allow to see the fitting of the three component hydraulic model as a two-objective optimization problem with eight parameters that can be approached with evolutionary computation.

A.1 Model Generalization

A schematic of the generalized form of the three component hydraulic model is depicted in Figure 1. Ignoring relations to lactate, carbohydrate or phosphocreatine, this work refers to the middle tank (A_nA in Morton’s schematic in Figure 5 of his review from 2006 [10]) as the anaerobic fast component AnF and the tank on the right (A_nL in Figure 5 of Morton’s review [10]) as the anaerobic slow component AnS. The left tank originally labeled with O for oxygen is renamed into the aerobic contribution Ae. This more general interpretation also allows to fully remove tube B, which was included in Morton’s work to account for early lactate levels in blood [8].

These are just slight adjustments but they represent a new perspective on the dynamics of the model. Rather than the originally intended concrete metabolic energy storages that have to be set

Permission to make digital or hard copies of part or all of this work for personal or classroom use is granted without fee provided that copies are not made or distributed for profit or commercial advantage and that copies bear this notice and the full citation on the first page. Copyrights for third-party components of this work must be honored. For all other uses, contact the owner/author(s).

GECCO '21 Companion, July 10–14, 2021, Lille, France

© 2021 Copyright held by the owner/author(s).

ACM ISBN 978-1-4503-8351-6/21/07.

<https://doi.org/10.1145/3449726.3459469>

up according to empirical measures, tanks now represent more abstract entities that allow to be interpreted as a combination of sources which can be fitted by optimizing an objective function.

A.2 Configurations

A configuration of our proposed adjusted three component hydraulic model entails component positions, sizes and capacities. In alignment to Figure 1, a configuration c for the model is defined as a collection of the following values,

$$c = \langle AnF, AnS, m^O, m^{AnS}, m^{AnF}, \phi, \theta, \gamma \rangle \quad (1)$$

where $\{AnF, AnS\}$ are tank capacities, $\{m^O, m^{AnS}, m^{AnF}\}$ are maximal flow capacities and $\{\phi, \theta, \gamma\}$ are distances to define tank and pipe positions.

A.3 Model Formalization

For simulations that allow to find an optimal configuration c via an evolutionary computation approach, the model needs to be formalized in a robust manner. All equations are detailed in correspondence to the notation depicted in Figure 1 and in accordance to approaches by Morton [6, 7, 9] and Sundström [13] who build upon Morton's work. Our simulations do not include efforts where the athlete has to work at the maximal intensity they can possibly sustain and therefore we do not cover Morton's and Sundström's limitations on maximal power output (limitations for a maximal p).

A simulation starts with the drainage of liquid to match power demands p . The simulation uses discrete time steps and the time difference between two time steps t and $t + 1$ is denoted as Δt . For the estimations of fill levels and flows for time step t , first the previous h_{t-1} is adapted according to the power demand p_t . This results in the intermediate level h_t^p .

$$h_t^p = h_{t-1} + \frac{p_t}{AnF} \cdot \Delta t \quad (2)$$

Now the liquids in tanks Ae and AnS react to the new fill level of AnF and flows are estimated. The contribution p^{Ae} from the Ae tank is estimated as follows.

$$p^{Ae} = \begin{cases} m^{Ae} \cdot \frac{h_t^p}{1-\phi}, & \text{if } 0 \leq h_t^p \leq (1-\phi). \\ m^{Ae}, & \text{otherwise.} \end{cases} \quad (3)$$

The maximal possible contribution m^{Ae} is scaled with the ratio of the fill level of AnF to $(1-\phi)$, which means the maximal flow is reached as soon as $h_t^p \geq (1-\phi)$. Because the size of Ae is infinite, liquid will never flow back into Ae and thus the interval of p^{Ae} is $[0, m^{Ae}]$.

Estimations of the flow from AnS to AnF or backwards from AnF to AnS are more sophisticated. The flow through this pipe is defined as p^{An} and, because liquid can refill AnS or flow out of it, the interval is $[-m^{AnF}, m^{AnS}]$. Let g^{max} be defined as the total height of AnS :

$$g^{max} = 1 - \theta - \gamma \quad (4)$$

To introduce possible flows more clearly, calculations are introduced in categories. The full Equation (8) for p_t^{An} , is the combination of Equation (5), Equation (6), and Equation (7) of this Appendix. Equation (5) describes cases in which no flow between AnS and

AnF happens and thus p_t^{An} equals 0.

$$p_t^{An} = \begin{cases} 0, & \text{if } h_t^p \leq \theta \\ & \text{and } g_{t-1} = 0. \\ 0, & \text{if } h_t^p \geq (1-\gamma) \\ & \text{and } g_{t-1} = g^{max}. \\ 0, & \text{if } h_t^p = (g_{t-1} + \theta). \end{cases} \quad (5)$$

In the first case, the tank AnS is full and the fill level of AnF is above the top of tank AnS . In the second case, the fill level of AnF is below the bottom end of AnS and AnS is empty. Finally, in the third one, the fill level of AnF is exactly at par with the fill level of AnS causing an equilibrium between both.

In Equation (6) cases in which liquid flows out of AnS into AnF are covered.

$$p_t^{An} = \begin{cases} m^{AnS} \cdot \frac{h_t^p - (g_{t-1} + \theta)}{g^{max}}, & \text{if } h_t^p > (g_{t-1} + \theta) \\ & \text{and } h_t^p < (1-\gamma). \\ m^{AnS} \cdot \frac{g^{max} - g_{t-1}}{g^{max}}, & \text{if } h_t^p \geq (1-\gamma) \\ & \text{and } g_{t-1} < g^{max}. \end{cases} \quad (6)$$

If the fill level of AnF is below the fill level of AnS and above the bottom end of AnS , the maximal possible flow is scaled according to the ratio of the difference between fill levels and the total height of AnS . Or, if the fill level of AnF is below the bottom end of AnS and AnS is not empty, the maximal flow is scaled according to the amount of remaining liquid to consider the pressure of remaining liquid in the tank.

Equation (7) describes the refilling flow—the flow back from AnF into AnS .

$$p_t^{An} = \begin{cases} m^{AnF} \cdot \frac{h_t^p - (g_{t-1} + \theta)}{g^{max}}, & \text{if } h_t^p < (g_{t-1} + \theta) \\ & \text{and } g_{t-1} > 0. \end{cases} \quad (7)$$

Here the fill level of AnF is above the fill level of AnS and AnS is not full, which causes liquid to flow back into AnS . The maximal flow m^{AnF} from AnF into AnS is scaled according to the ratio between the difference of fill levels and the height of AnS . Since h_t^p is smaller than $g_{t-1} + \theta$, the result will be negative, indicating that a re-flow into AnS happens.

As the result, the full equation for p_t^{An} is the combination of Equation (5), Equation (6) and Equation (7).

$$p_t^{An} = \begin{cases} 0, & \text{if } h_t^p \leq \theta \\ & \text{and } g_{t-1} = 0. \\ 0, & \text{if } h_t^p \geq (1-\gamma) \\ & \text{and } g_{t-1} = g^{max}. \\ 0, & \text{if } h_t^p = (g_{t-1} + \theta). \\ m^{AnS} \cdot \frac{h_t^p - (g_{t-1} + \theta)}{g^{max}}, & \text{if } h_t^p > (g_{t-1} + \theta) \\ & \text{and } h_t^p < (1-\gamma). \\ m^{AnS} \cdot \frac{g^{max} - g_{t-1}}{g^{max}}, & \text{if } h_t^p \geq (1-\gamma) \\ & \text{and } g_{t-1} < g^{max}. \\ m^{AnF} \cdot \frac{h_t^p - (g_{t-1} + \theta)}{g^{max}}, & \text{if } h_t^p < (g_{t-1} + \theta) \\ & \text{and } g_{t-1} > 0. \end{cases} \quad (8)$$

Having both flow values p_t^{Ae} and p_t^{An} of the current time step t , the tank fill levels of this time step are derived as:

$$h_t = h_t^p + \frac{p_t^{An} + p_t^{Ae}}{AnF} \cdot \Delta t \quad (9)$$

$$g_t = g_{t-1} + \frac{p_t^{An}}{AnS} \cdot \Delta t \quad (10)$$

These equations allow to estimate tank fill levels for each time step t throughout a simulation with possibly varying power demands p_t .

A.4 Handling Extreme Cases

Large values for Δt , or combinations of small parameter values for tanks sizes with large values for maximal flow rates can cause faulty estimations for p_t^{An} . These scenarios are not considered by Sundström [12, 13] or Morton [6–9] because Morton used differential equations on isolated test scenarios and Sundström's handcrafted simulation conditions seem to not cause situations in which such extreme values come into effect.

In order to make simulations robust in such cases, three limitations to the flow p^{An} are applied: In case Δt , m^{AnF} , or m^{AnS} are large, it can occur that p^{An} becomes larger than the remaining capacity of AnS or the negative p^{An} refills more liquid than AnS can store. For the case that not enough is remaining in AnS , p^{An} is capped to the remaining amount.

$$p_t^{An} = \min(p_t^{An}, (g^{max} - g_{t-1}) \cdot AnS) \quad (11)$$

Similarly, if p^{An} amounts to more re-flow into AnS than the available capacity, it is set to just fill AnS to the top.

$$p_t^{An} = \max(p_t^{An}, -g_{t-1} \cdot AnS) \quad (12)$$

Further, large Δt , m^{AnF} or m^{AnS} as well as AnF or AnS capacities can cause p^{An} to force a flow that overshoots the targeted equilibrium between both tank fill levels. Thus, the maximal flow m_t^{An} between both tanks is defined and limits p^{An} .

$$m_t^{An} = \frac{h_t^p - (g_{t-1} + \theta)}{\frac{1}{AnS} + \frac{1}{AnF}} \quad (13)$$

Since both p^{An} and m_t^{An} may be negative or positive, the limitation applies in the following manner:

$$p_t^{An} = \begin{cases} \max(m_t^{An}, p_t^{An}), & \text{if } p_t^{An} < 0. \\ \min(m_t^{An}, p_t^{An}), & \text{if } p_t^{An} > 0. \end{cases} \quad (14)$$

Applying these limits, model simulations stay robust even with extreme values and the model is ready to be fitted by an optimizer.

B OBJECTIVE FUNCTIONS

Two objectives capture how well a configuration c for the hydraulic model makes it recreate measured performances of a tested athlete. In this context the term fitness then describes how well the model reproduces the expected responses. Two fitness measures are to be optimized: energy expenditure and recovery. The ground truth performance measures are an athlete's finite energy reserve for work above critical power (W') and critical power (CP) as well as the group averaged recovery ratios that Caen et al. [3] observed on their participants.

B.1 Energy Expenditure

For the energy expenditure objective function, time to exhaustion estimations of the critical power concept [5] are compared to time to exhaustion estimations of the hydraulic model. Using the critical power concept, exercise intensities can be derived that lead to exhaustion after a given amount of seconds. A total of 12 intensities are estimated for the energy expenditure fitness. These intensities are the ones that are estimated to lead to exhaustion after 120, 130, 140, 150, 170, 190, 210, 250, 310, 400, 600, 1200 seconds. The three component hydraulic model with configuration c simulates constant exercise at these intensities. As soon as liquid flow out of the hydraulic model's tap p cannot sustain the demand anymore, exhaustion is reached and the total time to exhaustion is compared to the expected one. From these trials, a total of 12 differences between the expected amount of seconds until exhaustion and the simulated amount of seconds until exhaustion are derived. The normalized root mean squared difference of these is the error measurement to be minimized for the expenditure objective.

B.2 Energy Recovery

For an estimation of energy recovery capabilities of a hydraulic model, the recovery ratios summarized in Table 1 are used. The three component hydraulic model with configuration c simulates the same exercise protocol that Caen et al. [3] conducted to obtain their measurements.

Using the critical power concept [5], work rates that lead to theoretical exhaustion after 4 min (P4) and 8 min (P8) are derived. Using these intensities Caen et al. obtained the in Table 1 summarized recovery rates with a test setup that will be referred to as a work bout 1 (WB1) → recovery bout (RB) → work bout 2 (WB2) structure. It is conducted as follows: They let an athlete perform the first work bout (WB1) at a constant exercise intensity (in this case either P4 or P8) until the athlete cannot maintain this intensity anymore. This then assumes that W' is depleted. Afterwards immediately the recovery bout (RB) is started in which they switch to a much lower recovery intensity (in this case either 33% of CP (CP33) or 66% of CP (CP66)). This recovery phase prolongs for 2, 4 or 6 minutes and is followed by the second work bout (WB2) at the same intensity level as WB1 was conducted at. This second work bout also is stopped when the athlete cannot maintain the intensity anymore and the duration, i.e., time to exhaustion (TTE), are recorded for both work bouts. Because of the very limited recovery bout duration in-between both work bouts, the TTE of WB2 is bound to be shorter than the one of WB1, and the difference between both is considered to be the amount of W' balance (W'_{bal}) that was reconstituted during the RB.

As an example using Table 1, the first observation of the P4-CP33 line at 2 min represents a WB1 → RB → WB2 trial at the intensities P4 → CP33 → P4, where the recovery bout prolonged for 2 min. The duration of WB2 was 55% of the duration of WB1 and thus it is inferred that the athlete could retain 55% of their energy.

The three component hydraulic model with configuration c conducts the same protocol and exhaustion is the point where liquid flow out of tap p cannot meet the demand anymore. The normalized root mean squared error of these resulting 12 differences between

Table 1: Recovery ratios derived from [3]

	2 min	4 min	6 min
P4 - CP33	55 %	61 %	70.5 %
P4 - CP66	49 %	55 %	58 %
P8 - CP33	42 %	52 %	59.5 %
P8 - CP66	38 %	37.5 %	50 %

Note: Values are not precisely the ones from Caen et al. [3] and do not consider std errors. They are derived values to be simple for this proof of concept.

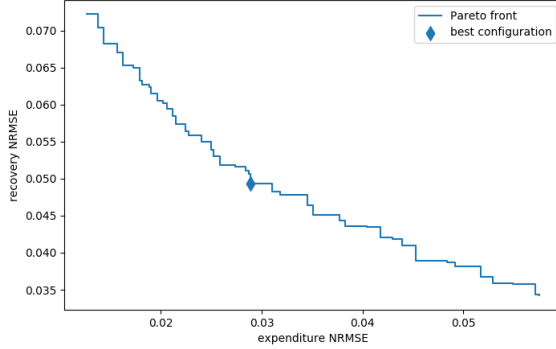


Figure 2: An exemplary Pareto front of an island. The best configuration on the Pareto front (blue diamond) is the one with minimal distance to point (0, 0) and marks the best possible trade-off between energy expenditure and recovery error.

observed recovery ratios and simulated recovery ratios is used as the error to be minimized for the recovery objective.

C THE EVOLUTIONARY ALGORITHM

A configuration c consists of eight real-valued parameters. A successful strategy to approximate an optimal configuration in such a search space is evolutionary computation [1, 2, 4]. The intention of this work is to provide a proof of concept that the proposed hydraulic model can be fitted to an athlete. Since a proof of concept is enough, the algorithm and parameter choices are not throughout fine tuned and we want to emphasize that much more room for parameter optimization and exploration of problem-specific algorithms is left for future work.

The defined objective functions evaluate expenditure and recovery as two distinct objectives, we chose the established Multi-Objective Evolutionary Algorithm with Decomposition (MOEA/D) approach as implemented in Pygmo [1, 11].

Two objectives are to be minimized: energy expenditure and recovery. Both objectives return a normalized root mean squared error of twelve measurements and are directly comparable. That allows to define the best trade-off between both dynamics to be the configuration on the Pareto front that has the smallest Euclidean distance to point (0, 0) (See example in Figure 2).

Table 2: Pygmo [1] default parameters for MOEA/D

parameter	value
weight_generation	'grid'
decomposition	'tchebycheff'
neighbors	20
CR	1
F	0.5
eta_m	20
realb	0.9
limit	2
preserve_diversity	true
seed	random

In initial experiments we obtained solutions in two categories: One heavily focused on the optimization of expenditure dynamics and the other one on the recovery dynamics. To improve generalization and to consistently find configurations that optimize both objectives, we couple MOEA/D with the asynchronous islands functionality of Pygmo [1]. That means several instances (one for each island) of the evolutionary algorithm are run isolated from each other. After a set number of generations, solutions from each of the island populations travel in-between islands. Then each algorithm continues to evolve their population, which now contains a few migrant solutions from the populations of the other algorithms. This step of evolving for a set number of generations and then exchanging solutions will be referred to as a cycle.

Except for the number of generations, population sizes, the number of islands, and the number of cycles, all parameters are at the default that Pygmo provides. Default parameters taken from Pygmo are summarized in Table 2.

Also for the asynchronous island approach we chose the default parameters of Pygmo in terms of migration types ('p2p') between islands and typologies ('fully connected'), but we do investigate various combinations of cycles (10,40,80), generations (10,20,30), population sizes (32,64), and numbers of islands (7,14,21). If the overall best fitness value of all island populations is not improved for more than 10 cycles, computations are stopped and the best solution of the last cycle is the returned result. The algorithm is run for ten times with each of the resulting parameter combinations. Results of all individual runs are summarized with the best (min), average (mean), and worst (max) distance result in Table 3. The configuration of the hydraulic model that resulted in the minimal distance (best configuration) is also denoted to give an idea of how sensitive the objectives are to changes in the 8 variables of a configuration.

Table 3: Grid search. Each parameter combination was run for 10 times.

							resulting best configuration parameters							
gens	cycles	population	islands	min	average	max	AnF	AnS	m^O	m^{AnS}	m^{AnF}	ϕ	θ	γ
10	10	32	7	0.0750	0.0896	0.1129	14887.19	78441.50	247.88	91.73	10.02	0.64	0.21	0.32
10	10	32	14	0.0732	0.0807	0.1020	16731.79	48023.39	246.03	113.48	9.60	0.70	0.01	0.29
10	10	32	21	0.0698	0.0766	0.0826	19526.85	78133.12	247.88	96.16	8.06	0.79	0.05	0.19
10	10	64	7	0.0707	0.0795	0.1028	18628.31	56881.67	247.51	108.59	8.15	0.76	0.02	0.22
10	10	64	14	0.0710	0.0730	0.0806	18325.37	53462.06	248.24	96.52	8.12	0.72	0.06	0.22
10	10	64	21	0.0704	0.0720	0.0756	18496.46	86583.43	248.30	91.07	8.91	0.78	0.09	0.20
10	40	32	7	0.0703	0.0745	0.0822	19074.54	255788.43	248.38	84.80	8.86	0.83	0.13	0.18
10	40	32	14	0.0705	0.0734	0.0894	18985.98	138678.84	248.24	85.07	8.09	0.80	0.12	0.19
10	40	32	21	0.0697	0.0707	0.0721	18664.83	94435.01	247.49	92.78	8.97	0.79	0.08	0.20
10	40	64	7	0.0695	0.0708	0.0749	19035.04	78738.60	248.04	94.84	8.08	0.78	0.07	0.20
10	40	64	14	0.0697	0.0704	0.0716	18082.63	47905.06	247.52	108.79	9.07	0.72	0.01	0.22
10	40	64	21	0.0694	0.0699	0.0703	19324.12	222108.58	247.90	81.11	9.01	0.81	0.14	0.18
10	80	32	7	0.0706	0.0737	0.0846	19061.94	98334.88	247.75	94.97	8.72	0.82	0.05	0.19
10	80	32	14	0.0698	0.0723	0.0769	17861.85	86634.11	247.95	90.63	9.53	0.75	0.11	0.22
10	80	32	21	0.0699	0.0713	0.0769	18917.47	144408.28	247.90	86.06	8.52	0.80	0.12	0.20
10	80	64	7	0.0698	0.0707	0.0751	19031.40	119081.83	248.05	85.09	8.81	0.79	0.11	0.19
10	80	64	14	0.0696	0.0706	0.0750	17958.82	67994.85	247.73	95.95	9.01	0.74	0.08	0.23
10	80	64	21	0.0697	0.0699	0.0704	17725.86	50325.31	247.26	107.09	9.27	0.72	0.02	0.23
20	10	32	7	0.0702	0.0775	0.1011	18922.50	69263.96	248.17	94.35	8.45	0.76	0.06	0.19
20	10	32	14	0.0709	0.0742	0.0805	17021.40	46888.56	247.03	106.46	9.81	0.68	0.04	0.26
20	10	32	21	0.0707	0.0731	0.0754	20195.32	101888.06	248.22	91.04	7.81	0.82	0.06	0.17
20	10	64	7	0.0700	0.0728	0.0768	18925.49	178845.77	248.02	85.65	9.63	0.80	0.13	0.19
20	10	64	14	0.0699	0.0703	0.0707	17642.03	79591.96	247.83	95.06	9.30	0.75	0.10	0.23
20	10	64	21	0.0695	0.0706	0.0725	18063.94	89567.17	247.71	91.83	9.48	0.75	0.11	0.22
20	40	32	7	0.0704	0.0745	0.0966	18240.97	62161.99	248.48	95.40	8.83	0.74	0.06	0.20
20	40	32	14	0.0701	0.0717	0.0742	20993.06	98680.10	248.57	86.20	7.18	0.82	0.07	0.15
20	40	32	21	0.0704	0.0713	0.0721	19882.77	132015.35	248.53	85.79	8.22	0.81	0.10	0.17
20	40	64	7	0.0695	0.0702	0.0734	17553.77	75082.95	247.60	91.18	9.70	0.73	0.11	0.23
20	40	64	14	0.0694	0.0698	0.0704	18287.25	50128.61	247.41	103.44	9.04	0.72	0.02	0.22
20	40	64	21	0.0691	0.0696	0.0698	18217.42	175251.33	248.05	85.18	9.26	0.78	0.15	0.21
20	80	32	7	0.0697	0.0713	0.0737	19431.50	160339.17	248.28	83.54	8.76	0.80	0.13	0.19
20	80	32	14	0.0700	0.0706	0.0740	18631.83	61995.02	247.59	99.87	8.95	0.76	0.04	0.21
20	80	32	21	0.0700	0.0705	0.0718	17613.36	56808.61	247.58	96.82	9.45	0.71	0.07	0.23
20	80	64	7	0.0695	0.0699	0.0704	19706.74	83704.90	248.09	93.96	8.12	0.80	0.06	0.18
20	80	64	14	0.0694	0.0698	0.0701	19214.76	65330.19	247.50	100.84	8.43	0.78	0.03	0.20
20	80	64	21	0.0695	0.0697	0.0701	18708.34	98318.64	247.66	90.08	9.14	0.78	0.10	0.20
30	10	32	7	0.0720	0.0782	0.0903	17042.00	185592.26	247.77	84.21	9.24	0.74	0.19	0.25
30	10	32	14	0.0701	0.0723	0.0753	18033.01	161795.47	247.53	85.22	9.75	0.78	0.14	0.21
30	10	32	21	0.0702	0.0715	0.0729	19264.53	77426.94	248.31	92.80	8.44	0.78	0.07	0.19
30	10	64	7	0.0694	0.0707	0.0733	19155.61	58966.01	248.05	101.65	7.88	0.77	0.03	0.20
30	10	64	14	0.0693	0.0700	0.0706	19544.79	70406.66	248.04	94.11	8.36	0.78	0.05	0.18
30	10	64	21	0.0693	0.0700	0.0711	18348.18	120883.19	247.66	85.21	9.11	0.77	0.13	0.21
30	40	32	7	0.0701	0.0720	0.0768	19898.17	136898.73	248.51	83.87	8.23	0.81	0.10	0.17
30	40	32	14	0.0700	0.0707	0.0715	18143.07	47370.24	247.84	105.76	9.07	0.71	0.02	0.21
30	40	32	21	0.0698	0.0702	0.0706	19269.44	57468.40	247.76	106.11	8.14	0.77	0.01	0.20
30	40	64	7	0.0691	0.0699	0.0716	18299.38	159976.90	247.83	84.20	9.24	0.78	0.15	0.21
30	40	64	14	0.0692	0.0695	0.0701	18581.79	109451.44	247.75	88.95	9.24	0.78	0.11	0.20
30	40	64	21	0.0692	0.0696	0.0702	19164.84	155545.77	248.26	83.53	8.15	0.79	0.14	0.20
30	80	32	7	0.0693	0.0715	0.0776	18397.78	48646.16	247.98	103.95	8.62	0.72	0.02	0.22
30	80	32	14	0.0701	0.0702	0.0704	17629.46	51157.57	247.16	106.93	9.23	0.72	0.03	0.24
30	80	32	21	0.0694	0.0702	0.0716	19211.40	75566.60	247.95	96.18	8.26	0.79	0.05	0.19
30	80	64	7	0.0695	0.0698	0.0702	18858.54	56032.86	247.37	103.52	8.99	0.75	0.02	0.20
30	80	64	14	0.0693	0.0696	0.0699	18295.58	115731.00	247.62	86.74	9.15	0.77	0.12	0.21
30	80	64	21	0.0692	0.0696	0.0699	18645.05	260070.20	248.17	81.43	8.96	0.79	0.16	0.20

REFERENCES

- [1] Francesco Biscani and Dario Izzo. 2020. A parallel global multiobjective framework for optimization: pagmo. *Journal of Open Source Software* 5, 53 (Sept. 2020), 2338. <https://doi.org/10.21105/joss.02338>
- [2] Thomas Bäck and Hans-Paul Schwefel. 1993. An overview of evolutionary algorithms for parameter optimization. *Evolutionary Computation* 1, 1 (March 1993), 1–23. <https://doi.org/10.1162/evco.1993.1.1.1>
- [3] Kevin Caen, Jan G. Bourgois, Gil Bourgois, Thibaut Van Der Stede, Kobe Vermeire, and Jan Boone. 2019. The reconstitution of W' depends on both work and recovery characteristics. *Medicine & Science in Sports & Exercise* 51, 8 (Aug. 2019), 1745–1751. <https://doi.org/10.1249/MSS.0000000000001968>
- [4] A.E. Eiben and J.E. Smith. 2015. *Introduction to evolutionary computing*. Springer Berlin Heidelberg, Berlin, Heidelberg. <https://doi.org/10.1007/978-3-662-44874-8>
- [5] David W. Hill. 1993. The critical power concept: a review. *Sports Medicine* 16, 4 (Oct. 1993), 237–254. <https://doi.org/10.2165/00007256-199316040-00003>
- [6] R. Hugh Morton. 1985. On a model of human bioenergetics. *European Journal of Applied Physiology and Occupational Physiology* 54, 3 (Sept. 1985), 285–290. <https://doi.org/10.1007/BF00426146>
- [7] R. Hugh Morton. 1986. On a model of human bioenergetics II: maximal power and endurance. *European Journal of Applied Physiology and Occupational Physiology* 55, 4 (Aug. 1986), 413–418. <https://doi.org/10.1007/BF00422743>
- [8] R. Hugh Morton. 1986. A three component model of human bioenergetics. *Journal of Mathematical Biology* 24, 4 (July 1986), 451–466. <https://doi.org/10.1007/BF01236892>
- [9] R. Hugh Morton. 1990. Modelling human power and endurance. *Journal of Mathematical Biology* 28, 1 (Jan. 1990), 49–64. <https://doi.org/10.1007/BF00171518>
- [10] R. Hugh Morton. 2006. The critical power and related whole-body bioenergetic models. *European Journal of Applied Physiology* 96, 4 (March 2006), 339–354. <https://doi.org/10.1007/s00421-005-0088-2>
- [11] Qingfu Zhang and Hui Li. 2007. MOEA/D: A Multiobjective Evolutionary Algorithm Based on Decomposition. *IEEE Transactions on Evolutionary Computation* 11, 6 (Dec. 2007), 712–731. <https://doi.org/10.1109/TEVC.2007.892759>
- [12] David Sundström, Peter Carlsson, and Mats Tinnsten. 2013. On optimization of pacing strategy in road cycling. *Procedia Engineering* 60 (2013), 118–123. <https://doi.org/10.1016/j.proeng.2013.07.062>
- [13] David Sundström, Peter Carlsson, and Mats Tinnsten. 2014. Comparing bioenergetic models for the optimisation of pacing strategy in road cycling. *Sports Engineering* 17, 4 (Dec. 2014), 207–215. <https://doi.org/10.1007/s12283-014-0156-0>